Conformational landscape and internal dynamics of limona ketone, a key oxidation product of limonene

Noureddin Osseiran, Annunziata Savoia, Pascal Dréan, Thérèse Huet, Manuel Goubet

Conformational landscape and internal dynamics of limona ketone, a key oxidation product of limonene

Noureddin OSSEIRAN, Annunziata SAVOIA, Pascal DRÉAN, Thérèse R. HUET, Manuel GOUBET*

Univ. Lille, CNRS, UMR 8523 - PhLAM - Physique des Lasers Atomes et Molécules, Lille 59000, France

Abstract

The rotational spectrum of limona ketone (4-acetyl-1-methyl-1-cyclohexene), a key oxidation product of limonene, was recorded in the gas phase using a Fourier transform microwave spectrometer coupled to a supersonic jet expansion over the 4 - 20 GHz range. To display a complete view of the conformational landscape of this relatively flexible system, the relative stability and inter-conversion barriers between conformers were explored by electronic structure calculations. The lowest energy equatorial conformer was detected, and its spectroscopic molecular parameters were determined from the analysis of the spectrum. The internal rotation of the methyl group attached to the aldehyde moiety was taken into account in the analysis. The internal dynamics of the methyl group within the acetyl moiety was quantitavely described. Experimental lines of both A and E symmetry were fitted to experimental accuracy, and the experimental barrier height of the methyl group internal rotation is discussed with the support of quantum chemical calculations.

Keywords: VOC, conformational landscape, internal rotation, microvawe spectroscopy, structure calculations

*Corresponding author
Email address: manuel.goubet@univ-lille.fr (Manuel GOUBET)

1. Introduction

Biogenic volatile organic compounds (BVOCs) are abundant in the Earth's atmosphere with a global emission by vegetation estimated at 760 $\mathrm{Tg(C)yr^{-1}}$ [1]. Many atmospheric BVOCs are terpenes, that primarily consist of two bonded isoprene subunits (C_5H_8). Limonene is the second major terpene released naturally in the atmosphere. It is mostly emitted from lemon trees, orange and citrus fruits. Its ozonolysis reaction is considered as one of the primary sources of the formation of secondary organic aerosols (SOA) [2, 3, 4, 5]. Because of its two chemically different double bonds, an endocyclic and an exocyclic double bond, the limonene ozonolysis has been the subject of many investigations [6, 7, 8, 9, 10, 11], using a variety of techniques, in order to identify the products of reaction and evaluate the thermodynamic and kinetic parameters. In particular, the first-generation products of the limonene ozonolysis may be unsaturated and exhibit high reactivity for further oxidation. Baptista *et al.* [6], using density functional methods (DFT), theoretically investigated the reaction steps of the ozonolysis with a focus on primary ozonide formation. The oxidation regime and SOA composition in limonene ozonolysis was also investigated [8]. Despite its importance as precursor of SOAs, only a few studies concerning the structure of limonene in the gas phase at the microwave accuracy are reported in the literature. Avilés-Moreno *et al.* [12] identified different conformations of limonene in the gas phase. Loru *et al.* [13] reported conformational flexibility of limonene oxide and characterized up to five conformers from the analysis of the pure rotation spectrum. More recently, Loru *et al.* [14] characterized axial conformers of limonene, carvone and perillaldehyde.

Limona ketone ($C_9H_{14}O$, 4-acetyl-1-methyl-1-cyclohexene, LK), referred also as keto-limonene, is one of the products of limonene oxidation [15]. Arey *et al.* [16] investigated products formed from the OH radical-initiated reactions of β-pinene and limonene in the presence of NO_x. By using gas chromatography with flame ionization detection (GC-FID), they analyzed the GC-FID traces and found two significant product peaks from d-limonene, one of them was

identified as LK. Gallimore *et al.* [17] investigated the oxidation of limonene in the Cambridge Atmospheric Simulation Chamber (CASC) and observed that LK is a short-lived oxidation product produced at low concentration and it is removed by further ozonolysis. LK is also identified as a product of ozonolysis of limonene. In 2005, Leungsakul *et al.* [18] proposed and tested experimentally a kinetic mechanism for predicting the formation of SOA from the reaction of limonene with O_3. Limononaldehyde was the major identified product followed by LK, keto-limonaldehyde, limononic acid and keto-limononic acid. Ham *et al.* [19] were able to detect five carbonyl compounds from limonene ozonolysis: LK, 7-hydroxy-6-oxo-3-(prop-1-en-2yl) heptanal, 3-isopropenyl-6-oxo-heptanal, 2-acetyl-5-oxohexanal and 3-acetyl-6-oxoheptanal. As for the first-generation products of limonene ozonolysis, LK exhibits high reactivity. It was found that it reacts with ozone in the Hyytiälä forest in spring time [20]. Moreover, Donahue *et al.* [21] showed that LK itself generates SOA with an efficiency that is statistically indistinguishable from α-pinene, probably due to the fact that they have a 1-methylcyclohexene moiety in common.

Fourier transform microwave (FTMW) spectroscopy in jet-cooled conditions is a powerful technique for investigating terpenoids, which are oxygenated derivatives of isoprene units. The first investigation of a group of terpenes using this technique was reported in 1978 [22]. The characterization of camphor using FTMW has been published more recently, in 2003 [23]. Since then, jet-cooled FTMW spectroscopy has been used to characterize a number of monoterpenes such as α-pinene [24], β-pinene [25], camphene [26], verbenone [27] and some of their oxidation products, namely perillaldehyde [28], nopinone [25], myrtenal [29] and fenchol [30]. Other monoterpenes obtained from oxydation and studied at microvawe accuracy are fenchone [31], menthol and (iso)menthone [32], thymol and carvacrol [33].

In this paper, we employed FTMW spectrometers to record the rotational spectrum of LK in jet-cooled conditions. The lowest energy conformer was detected and its molecular parameters are determined from the analysis of the spectrum. The internal rotation of the methyl group attached to the aldehyde

group is taken into account in the analysis. Experimental lines for both A and E states are fitted to instrumental accuracy and the experimental barrier height of the methyl group internal rotation is discussed with the support of quantum chemical calculations. In addition, the relative stability and inter-conversion barriers between conformers are explored by electronic structure calculations in order to display a complete view of the conformational landscape of this relatively flexible system.

2. Methods

2.1. Microwave spectroscopy

LK (referred as 4-acetyl-1-methyl-1-cyclohexene, 90 %) was purchased from Fluorochem and used without further purification. The pure rotation spectra of LK were recorded in the gas phase in the microwave region (3.8 - 19.3 GHz) using the Fabry-Perot Fourier-Transform microwave (FP-FTMW) technique coupled to a pulsed supersonic jet [34]. A heated nozzle [35] allowed to mix LK vapor with the carrier gas (neon) at an absolute backing pressure of about 0.4 MPa. A temperature of 343 K was found to optimize the signal-to-noise ratio (SNR) of recorded lines. The mixture was introduced into a Fabry-Perot cavity through a series 9 General Valve pin hole nozzle (1 mm) at a repetition rate of 1 Hz. Jet-cooled molecules (T_{rot} of a few K) were polarized within the supersonic expansion by a 2 µs microwave pulse. The free-induction decay (FID) signals were recorded using a heterodyne detection at 30 MHz and were digitized at a sampling rate of 120 MHz. After Fourier transformation of the average time domain signals, lines of the amplitude spectrum were observed as Doppler doublets due to the coaxial arrangement of the jet and the Fabry-Perot cavity. Each resonance frequency was measured as the average frequency of the two Doppler components. The number of recorded points was chosen so that the frequency grid was set to 1.8 kHz. Scans over several hundred of MHz were performed with a step of 250 kHz, each one consisting of 30 FIDs averaged and Fourier transformed, in order to roughly locate LK rotational lines. The experimen-

tal accuracy of the MW measured lines was estimated to 2 kHz. Examples of observed signals, both in low-resolution scan mode and high-resolution mode (insets), are shown in Figure 1. In particular, all lines were found split in two components, signature of an internal motion.

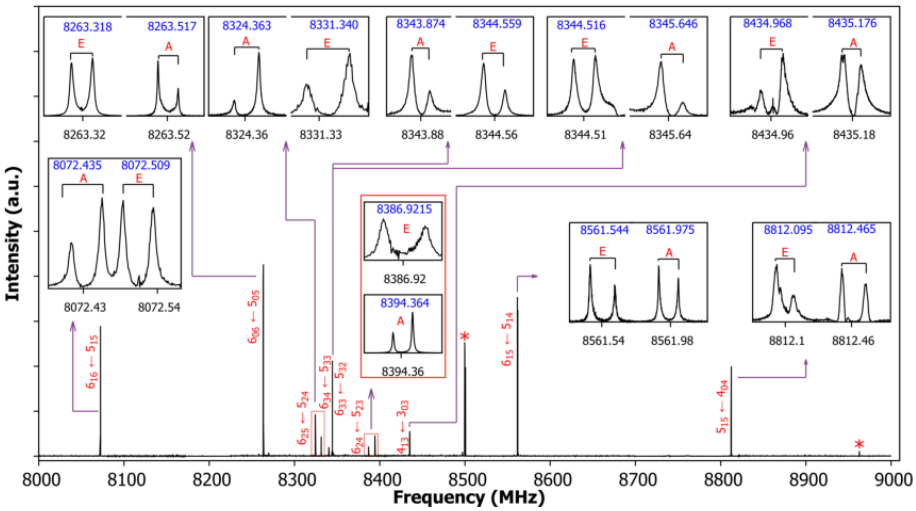

Figure 1: scan in low resolution mode (250 kHz steps) between 8000 and 9000 MHz of limona ketone, with insets at high resolution (1.8 kHz) for assigned peaks. Rotational lines are identified with $J_{K_a K_c}$ label and the split components associated with internal rotation are labeled with A/E symmetry. The star symbol indicates unassigned peaks.

2.2. Theoretical Calculations

Before the initial search of the rotational transitions, we performed quantum chemical calculations in order to obtain information on the relative energies of possible conformers and on their equilibrium geometries. All calculations were performed using the Gaussian 16 rev B.01 software package [36] on the high-performance computing cluster of PhLAM Laboratory. Møller–Plesset second order perturbation theory (MP2) [37, 38, 39, 40] as well as DFT methods, including Becke98 functional (B98) [41], Becke 3-parameter Lee–Yang–Parr functional (B3LYP) [42, 43, 44, 45] and Minnesota Functional (M06-2X) [46] were

used. Different basis sets were used throughout including: Dunning and coworkers augmented correlation consistent triple zeta (aug-cc-pVTZ) [47], Ahlrichs and coworkers split valence and triple zeta (def2TZVP) [48, 49] and Pople's 6-311++G(d,p) [50]. The quadratic synchronous transit (QST2) method [51], as implemented in Gaussian 16, was used at the MP2, B98, B3LYP and M06-2X levels of theory to calculate the energy of the transition state, and consequently the barriers of the methyl group internal rotation and the ring puckering motion (interconversion between equatorial and axial conformers, see hereafter). Concerning the acetyl group torsion, relaxed potential energy surface (PES) scans at the B98/aug-cc-pVTZ level were performed to characterize possible stable conformations. The geometry was optimized at each point of the scan (*i.e.* at each step of rotation of the dihedral angle containing the acetyl group). Geometries of the most stable conformers were subsequently fully optimized at the MP2, B98, B3LYP, M06-2X levels of theory. Vibrational frequencies (harmonic) and rotational constants (equilibrium) were calculated for each of the optimized geometries. A full list of the calculations, for all the predicted conformers, is given in the supplemental file.

3. Results and analyses

3.1. Conformational analysis

LK is a cyclic ketone having an endocyclic C-C double bond between C1 and C2 carbon atoms, an acetyl ($COCH_3$) group attached to a cyclohexene ring at carbon C4 and a methyl (CH_3) group attached to the ring at carbon C1. At C4, the acetyl group can be oriented in either equatorial (along the plane of cyclohexene ring) or axial (perpendicular to the plane of the ring) positions. Interconversion barrier between equatorial and axial is expected to be high (several tens of $kJ\,mol^{-1}$, see *e.g.* [52]), since it implies the acetyl group torsion in addition to the ring puckering motion. Indeed, QST2 calculations at the MP2/aug-cc-pVTZ result in a barrier height between most stable conformations

at equatorial and axial orientations of 20.9 kJ mol^{-1} (ZPE corrected at the harmonic level).

The torsion around the C4-C8 bond (acetyl group torsion), in both equatorial and axial orientations, can lead to different conformations displayed in Figure 2. To explore the conformational landscape, we performed a relaxed PES scan along the dihedral angle C5C4C8O10, with a step of 5°. Upon exploring the 1D potential energy surface (PES), we can see from Figure 3 that four equatorial conformers and two axial conformers are possible.

We named the equatorial conformers EQ1, EQ2, EQ3 and EQ4 and the axial conformers AX1 and AX2, from lowest to highest value of calculated energy. The calculated dihedral angle C5C4C8O10 value, at the MP2/aug-cc-pVTZ level of the theory, is equal to 272°, 325°, 141° and 103° for EQ1, EQ2, EQ3 and EQ4 and 19° and 236° for AX1 and AX2, respectively. The relative equilibrium structure energies, calculated with different methods and taking into account the zero point energy (ZPE) corrections at the harmonic level, along with rotation-vibration constants, are summarized in Figure 4.

The global minimum corresponds to the EQ1 conformer. Its optimized geometry at the MP2/aug-cc-pVTZ level of theory is presented in Figure 2a. Conformational relaxation within the supersonic expansion is expected when the conformational energy is above the barrier height. In our experimental conditions, the conformational energy of LK is equal to 2.8 kJ mol^{-1} (energy corresponding to a reservoir temperature of 343 K). A bare theoretical estimation of the barrier height is given by energy differences between minima and maxima from the relaxed scan of the PES along the acetyl group torsion (see Figure 3a). As shown in Figure 4, for EQ4 and EQ3, this difference ranges from 0.6 to 0.87 kJ mol^{-1} according to the different calculations performed. The barrier height from EQ4 to EQ3 is estimated to 0.53 kJ mol^{-1}, far below conformational energy and this barrier is a disputable point (see discussion hereafter), thus the EQ4 conformer is expected to relax to EQ3 conformer. Similarly, EQ2 is expected to relax to EQ1 since the energy difference ranges from 0.45 to 0.92 kJ mol^{-1} and the barrier height from EQ2 to EQ1 is estimated to 0.24 kJ mol^{-1}. The barrier

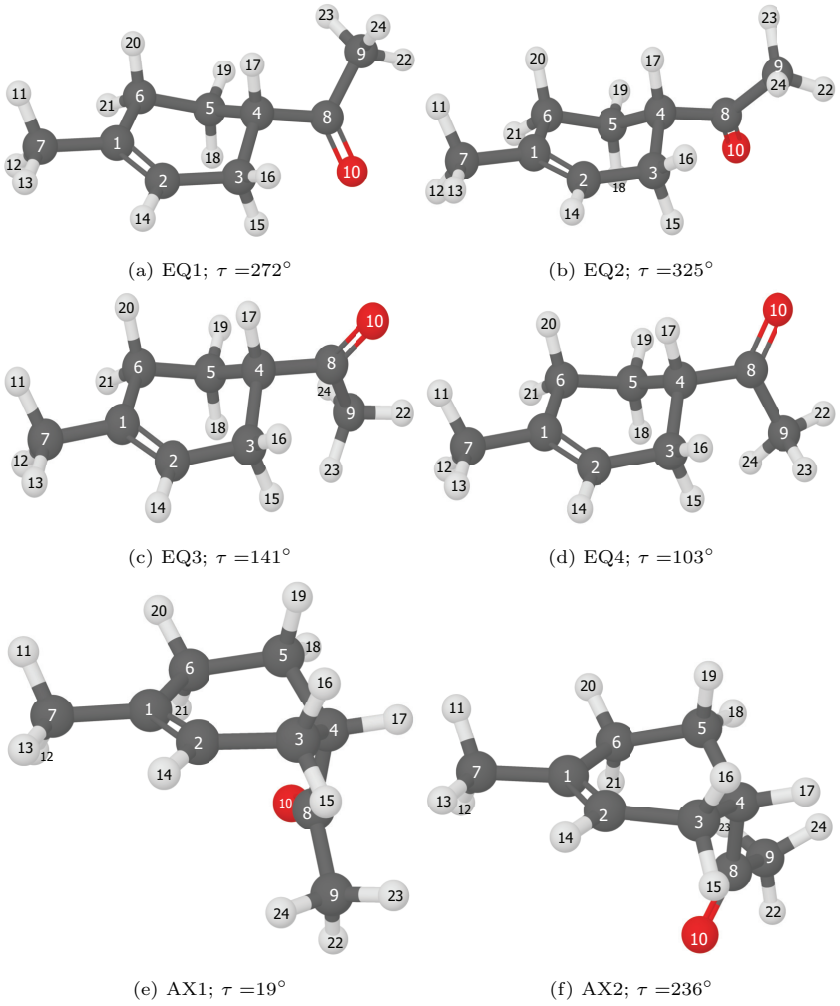

(a) EQ1; τ =272°

(b) EQ2; τ =325°

(c) EQ3; τ =141°

(d) EQ4; τ =103°

(e) AX1; τ =19°

(f) AX2; τ =236°

Figure 2: optimized geometries of all calculated stable equatorial and axial conformers of limona ketone at the MP2/aug-cc-pVTZ level of theory; τ represents the value of the dihedral angle C5C4C8O10.

height from EQ3 to EQ2 is estimated to 2.08 kJ mol^{-1}, so that another possible relaxation route goes from EQ4 to EQ1 passing by EQ2. Finally, the barrier height from EQ3 to EQ1 is estimated to 3.11 kJ mol^{-1}, slightly higher than conformational energy, thus relaxation from EQ3 to EQ1 is not expected, although possible. Such assumptions were verified for comparable systems: perillalde-

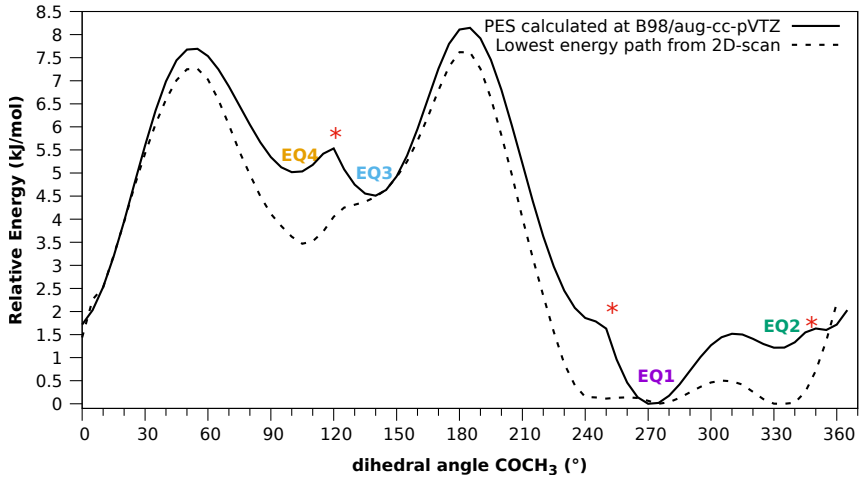

(a) Equatorial

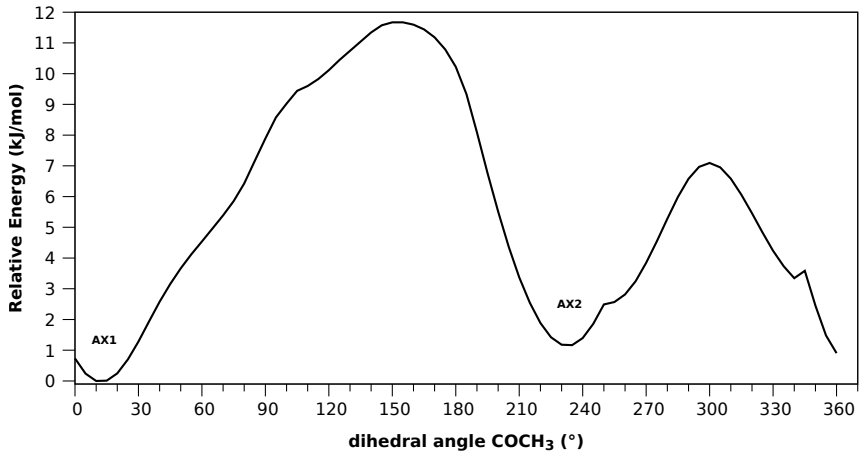

(b) Axial

Figure 3: Potential energy scan for the equatorial (a) and axial (b) configurations of limona ketone at the B98/aug-cc-pVTZ level of theory, with respect to the dihedral angle of the acetyl group $COCH_3$. In panel (a), surprising non-smooth points at certain angles are marked by an asterisk (*); the dash line represents the lowest energy path extracted from a 2-dimensional exploration of the potential energy surface (see in text section *4.2 conformational landscape* for details).

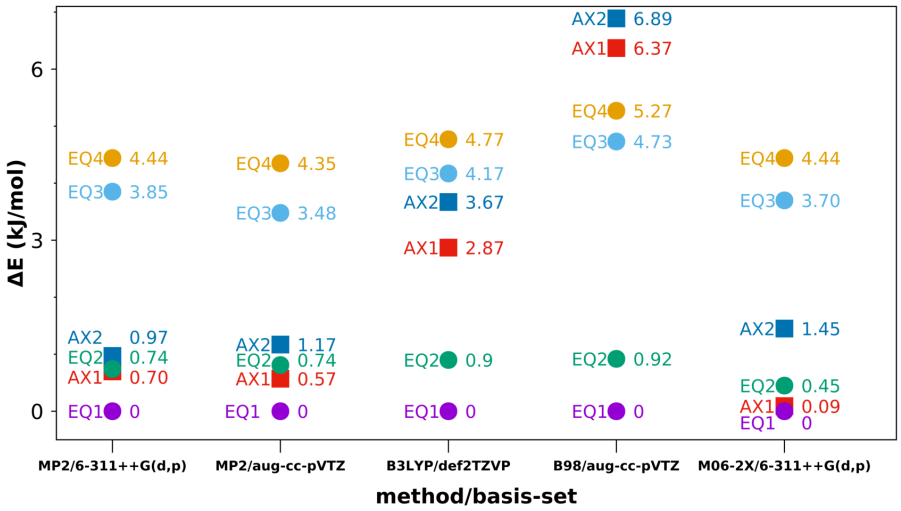

Figure 4: Relative energy (ΔE (kJ mol^{-1})) ordering of all calculated conformers of limona ketone from different methods and basis sets. Zero represents the lowest energy value. Values are ZPE corrected.

hyde, carvone and limonene [28, 12]. For axial conformers, the minimum energy structure corresponds to the AX1. Its optimized geometry at the MP2/aug-cc-pVTZ level is shown in Figure 2e. The AX2 conformer is not expected to relax to AX1 conformer because the barrier height is above the conformational energy value. In summary, based on energetic considerations, four conformers: EQ1, EQ3, AX1 and AX2 could be observed. A table provided in the supplemental file summarizes relevant molecular constants from all calculations methods used for the six conformers.

A noticeable feature in the experimental spectrum was observed. As we can see in Figure 1, each experimental line had a neighboring line with similar intensity, splittings ranging from few kHz to few MHz. This splitting pattern is characteristic of an internal rotation motion, such as the torsion of a methyl group which changes the degeneracy of the rotational levels and splits them into two symmetry states: A and E. Thus, each transition will be split into two lines of equal intensity. This splitting is further discussed hereafter.

3.2. Spectral analysis

LK in EQ1 conformation is a prolate asymmetric rotor with Ray's asymmetric parameter having a value of $\kappa = -0.935$. Preliminary predictions of the spectrum were made based on a semi-rigid rotor Hamiltonian (Watson's A-reduction) from the rotational constants calculated at different levels of theory, using SPFIT/SPCAT program suite [53]. The assignment started by fitting intense lines observed in the scan to predicted transitions, and then including gradually series of lines with increasing quantum numbers and different variations of K_a and K_c. Lines of different transition types were added, as well as Q-branch transitions. In the following, the notations used include information about the assigned lines. The a,b,c exponents represent the transition type with respect to dipole components in the principal axes. The R or Q symbols correspond to R- and Q-branch transitions ($\Delta J = 1$ and $\Delta J = 0$), respectively. The two subscript components represent the ΔK_a and ΔK_c values. A set of 107 lines including 45 of a-type (all of them being $^{a}R_{01}$), 37 b-type (17 $^{b}R_{11}$, 1 $^{b}R_{01}$, 14$^{b}R_{1-1}$, 4 $^{b}R_{-11}$, 1 $^{b}R_{10}$) and 25 c-type (19 $^{c}R_{10}$, 1 $^{c}R_{1-1}$, 5 $^{c}R_{1-2}$) up to J = 13 and $K_a = 4$ was finally obtained, corresponding to a consistent set of A symmetry transitions. The line intensities of the different transition types were in accordance with the calculated dipole moment components ($|\mu_a| < |\mu_c| < |\mu_b|$, see Table 1 for calculated values). The root-mean-square (RMS) value of the fit is 1.32 kHz, in agreement with the instrumental accuracy. The fitted values of the rotational and quartic distortion constants are summarized in Table 1. The values are in good agreement with calculated constants, with the difference ranging between 0.3 and 1.1 %. This magnitude of differences is expected when comparing *ground state* experimental values with *equilibrium* theoretical values.

Table 1: **Experimental and calculated rotational and quartic centrifugal distortion constants, of limona ketone lowest energy equatorial conformer (EQ1), along with other spectroscopic parameters.**

Parameters	Exp. value (SPFIT)	Exp.value (XIAM)	MP2[a]	MP2[b]	B3LYP[c]	B98[b]	M06-2X[a]
A (MHz)	3159.788 66(11)	3159.509 939(292)	3151.24	3173.01	3184.07	3169.26	3175.23
B (MHz)	735.407 909(45)	735.390 027(96)	732.36	741.18	734.05	727.51	738.52
C (MHz)	653.518 570(52)	653.512 896(91)	660.44	662.23	656.74	651.66	656.66
Δ_J (kHz)	0.030 16(18)	0.030 581(395)	0.03	0.03	0.03	0.03	0.02
Δ_{JK} (kHz)	0.0571(24)	0.052 08(312)	0.06	0.07	0.07	0.07	0.06
Δ_K (kHz)	0.3659(86)	0.3362(158)	0.44	0.40	0.38	0.39	0.37
δ_J (kHz)	0.001 516(74)	0.002 012(238)	0.003	0.001	0.002	0.002	0.001
δ_K (kHz)	0.834(21)	0.8315(260)	0.63	0.56	0.63	0.60	0.51
V_3 (cm^{-1})	···	298.39(25)	207.12	183.24	178.27	238.89	125.52
ϵ (rad)	···	2.615 051(959)	2.36	2.32	2.35	2.34	2.39
δ (rad)	···	2.230 887(506)	2.13	2.08	2.09	2.08	2.09
Dpi2- (kHz)	···	−317622(807)	···	···	···	···	···
F_0 (GHz)	···	163.561(115)	···	···	···	···	···
RMS[d] (kHz)	1.32	3.36	···	···	···	···	···
N[e]	101	214	···	···	···	···	···
μ_a[f] (D)	···	···	1.2	1.2	1.2	1.2	1.3
μ_b[f] (D)	···	···	1.9	1.9	2.0	2.0	2.1
μ_c[f] (D)	···	···	1.8	1.7	1.8	1.8	1.7

[a]6-311++G(d,p) basis set; [b]aug-cc-pVTZ basis set; [c]def2TZVP basis set; [d]root mean square value of observed - calculated line frequencies; [e]number of lines used in the fit: only A symmetry components with SPFIT, both A and E symmetry components with XIAM; [f]dipole moment component in the principal axes system

A more detailed look shows that the A constant is best calculated using the MP2 method, whereas the B and C constants are better predicted with the DFT (B98 and B3LYP) methods. Concerning quartic centrifugal distortion constants, and because of the limited range of values of J, K_a and K_c accessible in the microwave region, their deviations from theoretical calculations are relatively more important, but their sign and order of magnitude are consistent as usually expected.

In order to address the observed splitting, we should consider the two methyl groups that are present in LK: one attached to C1 atom and the other attached to the carbonyl moiety of the acetyl group. We named them M1 and M2, respectively. The magnitude of the splitting depends on the barrier height of the methyl torsion. Thus, the barrier height (V_3) associated to M1 and M2 internal rotations was calculated at different levels of theory using the QST2 method. For M1, we obtained a value of $790\,\mathrm{cm}^{-1}$ at the MP2/6-311++G(d,p) level of theory. From experience, such barrier height higher than roughly $500\,\mathrm{cm}^{-1}$ is expected to cause splitting on the lowest energy levels ranging from several kHz to few tens of kHz which are too small to be observed at our instrumental resolution. For M2, V_3 varies in a wide range from $125\,\mathrm{cm}^{-1}$ to $240\,\mathrm{cm}^{-1}$ depending on the method used. The values obtained are summarized in Table 1. A barrier height of such magnitude is considered to be intermediate, and a splitting into two components of A and E symmetry of each observed transition expected to be observed, ranging from few kHz to few hundreds of MHz. Hence, the splitting due to internal rotation of M2 was considered in the spectral analysis.

The XIAM program [54], which treats the internal rotation motion, was used to perform an effective fit of A and E transitions observed in the spectrum. XIAM was chosen because it uses a simple Hamiltonian based on Watson's 1^{st} order Hamiltonian, and it usually results in reliable fits in the case of medium-to-high internal rotation barriers as in the present case of LK EQ1. Starting from predictions based on the fitted parameters with SPFIT, and the ZPE corrected barrier height calculated at the MP2/aug-cc-pVTZ level, experimental frequencies of the E components have been assigned and fitted in addition to the

A components that have been previously assigned. The final XIAM fit includes 214 lines (78 a-type including 22 $^{a}R_{01}$ and 56 $^{a}R_{0-1}$, 82 b-type including 16 $^{b}R_{-1-1}$, 10 $^{b}R_{1-1}$, 22 $^{b}R_{-11}$ and 34 $^{b}Q_{-11}$ as well as 54 c-type including 40 $^{c}R_{-10}$, 6 $^{c}Q_{10}$, 2 $^{c}Q_{-1-2}$ and 6 $^{c}Q_{-10}$) up to $J = 13$ and $K_a = 4$ and shows a RMS deviation of 3.36 kHz. A complete list of assigned transitions is available in the supplemental file. The V_3 potential energy parameter, the angles δ (angles between the internal rotation axis and the principal axis z) and ϵ (angle between the principal axis x and the projection of the internal rotation axis onto xy-plane) and the internal rotation constant F_0 are fitted. The use of the "Dpi2-" empirical parameter that is programmed in XIAM [55] (internal rotation-overall rotation distortion parameter) was necessary to reach instrumental accuracy. Values from the best fit are listed in Table 1.

The experimentally deduced rotational constants are compared to the calculated ones in Table 1. Noticeably, the rotational constants obtained with XIAM, by fitting both A and E symmetry components, are close to those obtained from the semi-rigid rotor fit, by fitting A symmetry components only, and they are still in good agreement with calculations. Individual errors also depend on the method used.

4. Discussions

4.1. Internal rotation motion

The V_3 value is theoretically underestimated whatever the method used (see Table 1). In addition, the use of the Dpi2- parameter is unexpected when fitting centimeter-wave data only. Such discrepancy might be explained accounting for the fact that XIAM program refers to an isolated system where only the methyl group rotates, whereas all the system is relaxed and optimized in theoretical calculations. In this context, the barrier height was then calculated at the MP2/aug-cc-pVTZ level of theory with an "adiabatic" path where only the methyl group was rotated and all other atoms were kept fixed at equilibrium structure. The obtained "adiabatic" value V_3^{ad} is 442 cm^{-1}. As a result, the

experimental barrier height $V_3^{exp} = 298\,\mathrm{cm}^{-1}$ is almost at the center of the range obtained from the "relaxed" value $V_3^{rel} = 183\,\mathrm{cm}^{-1}$ to the "adiabatic" value ($V_3^{rel} < V_3^{exp} < V_3^{ad}$). This result indicates that an interaction exists between M2 internal rotation and the skeleton of LK. Such effect was already evidenced, for example in the case of methacrolein [56], methylglyoxal [57] or 2-nitrotoluene [58]. Another noticeable example of similar situation was observed in 2-Acetyl-5-methylfuran [59]. As a consequence, in the absence of a model taking into account an interaction between large amplitude motions, only an effective fit can be performed to reach instrumental accuracy, by using second or higher order terms (Dpi2- in the present case) in the isolated internal rotation hamiltonian. Other arguments pointing toward an interaction between internal motions are developed in the following.

4.2. Conformational landscape

The study of relaxed potential energy scans (Figure 3) was the first step in exploring the conformational landscape of LK. The scans, for both axial and equatorial conformers, showed some non-smooth points at certain angles, that can be seen as small bumps in the curve (as marked by a * in Figure 3). This was also pointed out in the case of 2-Acetyl-5-methylfuran [59]. A recheck of these points was necessary to understand whether they are artifacts from the calculations or they signify a physical interaction. Focusing on the equatorial configuration, one of these points leads to the assumption that we might have two minima around 120°, thus expecting EQ2 and EQ3 conformers, when in fact we might have just one minimum. A primary check was to calculate the PES scans using different combinations of method and basis sets and particularly have a deeper look around these points with smaller steps (1°). The bumps occurred through all calculations (see figure provided in supplemental file). Second, we followed the optimized geometry at each point of the scan to check any sudden change in geometry. We noticed that, for example, when the dihedral angle of the acetyl group is around 119°, M2 unexpectedly jumps of about 40°. This movement is shown in figure 5. When we compared the two geometries,

the hydrogen atoms of M2 seem to mirror themselves through this rotation by a "symmetry" plane of LK skeleton, suggesting that the optimization process tries to lower the steric hindrance by suddenly switching to an almost iso-energetic geometry. This movement can be observed similarly at the other bumps for both axial and equatorial conformers.

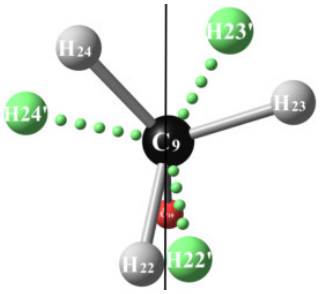

Figure 5: Geometry of the methyl group M2 (CH_3) of equatorial conformers of limona ketone at an acetyl group ($COCH_3$) orientation of 119° (gray bonds) and 120° (green dashed bonds). The calculated angle of sudden rotation is about 40°

As this observation is not enough to understand whether these bumps have a physical significance or not, and driven by the fact that the experimental barrier height of M2 does not match the calculated value with two approaches (see previous subsection), a two-dimensional PES exploration has been performed. Indeed, as pointed out in a recent study [58], an iso-surface can be used to visualize such effects. The PES was calculated across two relevant dihedral angles, C5C4C8C10 and C4C8C9H22 corresponding to the rotation of the acetyl and M2 groups, respectively, by means of relaxed scans of 5° steps. The PES and its iso-surface are shown in Figure 6a and 6b , respectively. The overall PES displays a smooth behavior without any break from one point to the next. Along M2 rotation (*i.e.* when acetyl dihedral angle is fixed), curves look like a standard 3-fold potential as expected. Along acetyl rotation, curves qualitatively agree with the fully relaxed scan (Figure 3a). Without interactions between the two movements, one would expect a PES with horizontal and vertical orientations of valleys which means that one group rotates without influencing the other.

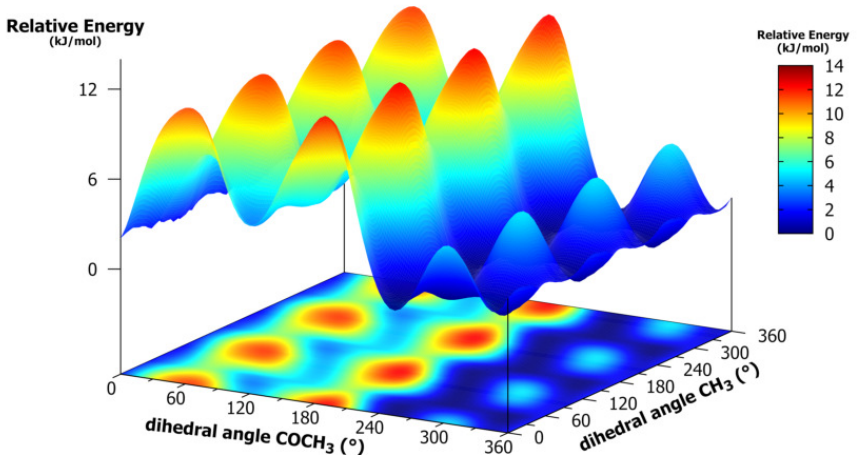

(a) 3D view.

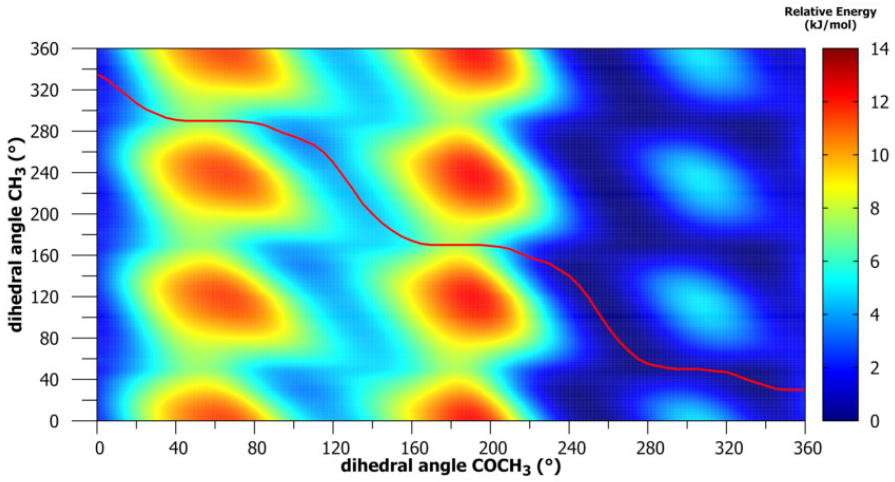

(b) Isosurface view.

Figure 6: 2-dimensions potential energy surface of limona ketone in equatorial configuration with respect to $COCH_3$ and CH_3 rotations, displayed in (a) 3D view and (b) isosurface plot. In panel (b), The red line represents the following of the path with the lowest energy value.

However, the present iso-surface clearly displays a diagonal orientation of valleys (see Figure 6b) which is, on the contrary, an evidence of an interaction between

these two rotations. Indeed, starting from one minimum, only a concerted torsional motion is possible to reach another relative minimum (*i.e.* by roughly following dark blue points on the iso-surface). Noticeably, complete rotations of M2 to reach an equivalent position (*i.e.* rotations of 120°) are achieved at the acetyl group angles where bumps are observed in the relaxed scan. Therefore, we followed quantitatively the minimum energy path in the 2D PES: starting from a minimum position (acetyl=275°; M2=60°), we took the closest lowest energy point on the next PES slice (at acetyl angle +5°) and so on until complete rotation of the acetyl group. The obtained PES cut is shown in Figure 3a where it is compared to the fully relaxed scan. First, one can clearly see that bumps are no longer present in the cut, leading to the conclusion that these bumps have no significant physical meaning and they are due to calculation "artifacts" correlated with the relaxed scan procedure. Second, EQ3 no longer exists in the cut, suggesting that EQ3 and EQ4 are rather "mirror images" of themselves than two different stable conformations (see Figures 2c and 2d). Third, the well around EQ1 and EQ2 appears very flat in the minimum energy path curve. One explanation could come from the fact that following a minimum path in a 2D surface only takes into account constraints between the two followed elements, and does not take into account the constraints with the rest of the molecule, whereas a fully relaxed scan does. For example, when rotating the acetyl group at fixed steps, some electrostatic repulsion or perturbations of the overlapping molecular orbitals might be compensated by an "over-rotation" of the methyl group which would not have occurred in a system fully relaxed. Finally, the most realistic potential energy curve of the internal rotation of the acetyl group should be somewhere in between, probably closer to the fully relaxed scan but without bumps. In any case, this behavior can be qualitatively used to confirm the presence of interactions between M2 internal rotation and a LK skeleton movement such as acetyl rotation, which explains the disagreement between the experimental barrier height (V_3 parameter) and its theoretical estimation using two different approaches ("adiabatic" and "relaxed" energy curves), as well as the unexpected use of the Dpi2- parameter.

4.3. Search for higher energy conformers

After analysis of LK EQ1 spectrum, taking into account line splitting due to the internal rotation of the methyl group M2, some observed lines remain unassigned. Although many of them are very weak thus most probably belong to ^{13}C isotopic species in natural abundance (whose analysis is out of the scope of the present study), few of them are strong enough to deserve further investigation (weak lines of EQ1 have SNR from 5 to 99, whereas one unassigned line has a SNR of 750, the few others having SNR from 10 to 90). The most reasonable guess is that they might arise from the other conformers of LK, in particular AX1, EQ2 and AX2 which are relatively close in energy to EQ1 (see Figure 4). Indeed, the Boltzmann distribution at sample temperature (343 K) over all five conformers based on MP2 relative energies would give an initial sample (before expansion in the jet) composed of about 28 % of EQ1, 22 % of AX1, 18 % of AX2, 18 % of EQ2 and 14 % of EQ3/EQ4. However, all attempts to perform a fit at instrumental accuracy with a set of molecular parameters corresponding to LK conformers were unsuccessful. This tends to correlate with our initial assumption of a strong relaxation to EQ1 within our jet expansion.

Then, a search for the presence of precursor molecules and/or impurities in the sample was undertaken, starting from the LK synthesis process. LK is synthesized using a Diels–Alder reaction of isoprene and methyl vinyl ketone on dry silica gel [21]. The rotational constants of isoprene [60, 61] and methyl vinyl ketone [62] being well known, we tried to assign unidentified lines to isoprene and/or metyl vinyl ketone, but here again without success.

During the synthesis of LK, the 4-acetyl-2-methylcycloxene, a meta substituted isomer, was observed [21]. Therefore, calculations at the MP2/6-311++G(d,p) level were performed to identify the possible conformers and to obtain the rotational constants of the most stable one. One more time, attempts to attribute unidentified signals to this molecule were unsuccessful.

Finally, searches into splatalogue spectroscopic database [63] were undertaken focusing on spectra of known molecules similar to LK, with respect to the C_8O_{10} double bond, such as acetone or acetaldehyde, unsuccessfully. As a

consequence of all these numerous attempts, we believe that the assignment of these few lines is much more challenging than expected and falls beyond the scope of the work presented here.

5. Conclusion

In this paper, a microwave study of limona ketone is presented through a combined experimental and theoretical approach. We use a Fourier transform microwave spectrometer coupled to a supersonic jet expansion over the 3.8 - 19.3 GHz range. Considering the theoretical relative energy values, four conformers were expected, but only one, the most stable from calculated energies, is observed. This is most probably due to conformational relaxation upon our supersonic expansion conditions. The spectrum clearly shows line splittings characteristic of an internal rotation motion, identified to the methyl group attached to the carbonyl moiety of the acetyl group. Both SPCAT/SPFIT and XIAM program suites are employed in a sequential method: a preliminary fit to the A symmetry transitions using SPFIT followed by a fit of both A and E symmetry transitions using XIAM. The experimentally deduced value of the barrier to internal rotation is $V_3^{exp} = 298$ cm^{-1}. Besides the barrier height value, the analysis of the internal rotation provided information about the interaction of the methyl group within the molecular framework. Indeed, although the agreement between theoretical and experimental internal rotation parameters is only qualitative, a two-dimensional exploration of the potential energy surface clearly evidences an interaction between the methyl group internal rotation and a skeleton movement, that is the acetyl group torsion, which explains the discrepancy. Moreover, a standard unidimensional scan of the PES displayed some surprising features (discontinuities and an unexpected conformer EQ3), which have been identified as computational artifacts thanks to a more detailed 2D exploration. The methodology proposed in the present work should be of interest for other compounds containing acetyl moiety. Attempts to identify the higher energy conformers in the spectrum were unsuccessful, confirming the

assumption of a strong relaxation to the most stable conformer EQ1 within the jet expansion. Finally, from the atmospheric application point of view, the present data can provide the fundamentals for future studies of microsolvation effect and/or aggregation of limona ketone.

Acknowledgement

The present work was funded by the French ANR Labex CaPPA through the PIA under contract ANR-11-LABX-0005-01, by the Regional Council Hauts de France, by the European Funds for Regional Economic Development (FEDER) and by the French Ministère de l'Enseignement Supérieur et de la Recherche. It is a contribution to the CPER research Project CLIMIBIO.

References

[1] K. Sindelarova, C. Granier, I. Bouarar, A. Guenther, S. Tilmes, T. Stavrakou, J.-F. Müller, U. Kuhn, P. Stefani, W. Knorr, Global data set of biogenic voc emissions calculated by the megan model over the last 30 years, Atmospheric Chemistry and Physics 14 (17) (2014) 9317–9341. doi:10.5194/acp-14-9317-2014.

[2] A. Calogirou, B. R. Larsen, D. Kotzias, Gas-phase terpene oxidation products: A review, Atmospheric Environment 33 (9) (1999) 1423–1439. doi:10.1016/S1352-2310(98)00277-5.

[3] S. Koch, R. Winterhalter, E. Uherek, A. Kolloff, P. Neeb, G. K. Moortgat, Formation of new particles in the gas-phase ozonolysis of monoterpenes, Atmospheric Environment 34 (23) (2000) 4031–4042. doi:10.1016/S1352-2310(00)00133-3.

[4] R. Atkinson, J. Arey, Gas-phase tropospheric chemistry of biogenic volatile organic compounds: A review, Atmospheric Environment 37 (2003) 197–219. doi:10.1016/S1352-2310(03)00391-1.

[5] W. Ahmad, C. Coeur, A. Cuisset, P. Coddeville, A. Tomas, Effects of scavengers of criegee intermediates and oh radicals on the formation of secondary organic aerosol in the ozonolysis of limonene, Journal of Aerosol Science 110 (2017) 70–83. doi:https://doi.org/10.1016/j.jaerosci.2017.05.010.

[6] L. Baptista, R. Pfeifer, E. C. da Silva, G. Arbilla, Kinetics and Thermodynamics of Limonene Ozonolysis, The Journal of Physical Chemistry A 115 (40) (2011) 10911–10919. doi:10.1021/jp205734h.

[7] S. E. Sbai, B. Farida, Photochemical aging and secondary organic aerosols generated from limonene in an oxidation flow reactor, Environmental Science and Pollution Research 26 (18) (2019) 18411–18420. doi:10.1007/s11356-019-05012-5.

[8] Y. Gong, Z. Chen, H. Li, The oxidation regime and SOA composition in limonene ozonolysis: Roles of different double bonds, radicals, and water, Atmospheric Chemistry and Physics 18 (20) (2018) 15105–15123. doi:10.5194/acp-18-15105-2018.

[9] D. Johnson, G. Marston, The gas-phase ozonolysis of unsaturated volatile organic compounds in the troposphere, Chemical Society Reviews 37 (4) (2008) 699–716. doi:10.1039/B704260B.

[10] D. F. Zhao, M. Kaminski, P. Schlag, H. Fuchs, I.-H. Acir, B. Bohn, R. Häseler, A. Kiendler-Scharr, F. Rohrer, R. Tillmann, M. J. Wang, R. Wegener, J. Wildt, A. Wahner, T. F. Mentel, Secondary organic aerosol formation from hydroxyl radical oxidation and ozonolysis of monoterpenes, Atmospheric Chemistry and Physics 15 (2) (2015) 991–1012. doi:10.5194/acp-15-991-2015.

[11] Å. K. Watne, J. Westerlund, Å. M. Hallquist, W. H. Brune, M. Hallquist, Ozone and OH-induced oxidation of monoterpenes: Changes in the thermal properties of secondary organic aerosol (SOA), Journal of Aerosol Science 114 (2017) 31–41. doi:10.1016/j.jaerosci.2017.08.011.

[12] J. R. A. Moreno, T. R. Huet, J. J. L. González, Conformational relaxation of S-(+)-carvone and R-(+)-limonene studied by microwave Fourier transform spectroscopy and quantum chemical calculations, Structural Chemistry 24 (4) (2013) 1163–1170. doi:10.1007/s11224-012-0142-8.

[13] D. Loru, M. M. Quesada-Moreno, J. R. Avilés-Moreno, N. Jarman, T. R. Huet, J. J. López-González, M. E. Sanz, Conformational Flexibility of Limonene Oxide Studied By Microwave Spectroscopy, ChemPhysChem 18 (3) (2017) 274–280. doi:10.1002/cphc.201600991.

[14] D. Loru, A. Vigorito, A. F. M. Santos, J. Tang, M. E. Sanz, The axial/equatorial conformational landscape and intramolecular dispersion: New insights from the rotational spectra of monoterpenoids, Physical Chemistry Chemical Physics 21 (47) (2019) 26111–26116. doi:10.1039/C9CP05264J.

[15] V. Librando, G. Tringali, Atmospheric fate of OH initiated oxidation of terpenes. Reaction mechanism of α-pinene degradation and secondary organic aerosol formation, Journal of Environmental Management 75 (3) (2005) 275–282. doi:10.1016/j.jenvman.2005.01.001.

[16] J. Arey, R. Atkinson, S. M. Aschmann, Product study of the gas-phase reactions of monoterpenes with the OH radical in the presence of NO x, Journal of Geophysical Research: Atmospheres 95 (D11) (1990) 18539–18546. doi:10.1029/JD095iD11p18539.

[17] P. J. Gallimore, B. M. Mahon, F. P. H. Wragg, S. J. Fuller, C. Giorio, I. Kourtchev, M. Kalberer, Multiphase composition changes and reactive oxygen species formation during limonene oxidation in the new Cambridge Atmospheric Simulation Chamber (CASC), Atmospheric Chemistry and Physics 17 (16) (2017) 9853–9868. doi:10.5194/acp-17-9853-2017.

[18] S. Leungsakul, M. Jaoui, R. M. Kamens, Kinetic Mechanism for Predicting Secondary Organic Aerosol Formation from the Reaction of d-Limonene

with Ozone, Environmental Science & Technology 39 (24) (2005) 9583–9594. doi:10.1021/es0492687.

[19] J. E. Ham, J. C. Harrison, S. R. Jackson, J. R. Wells, Limonene ozonolysis in the presence of nitric oxide: Gas-phase reaction products and yields, Atmospheric Environment 132 (2016) 300–308. doi:10.1016/j.atmosenv.2016.03.003.

[20] H. Hellén, H. Hakola, A. Reissell, T. M. Ruuskanen, Carbonyl compounds in boreal coniferous forest air in Hyytiälä, Southern Finland, Atmospheric Chemistry and Physics 4 (7) (2004) 1771–1780. doi:10.5194/acp-4-1771-2004.

[21] N. M. Donahue, J. E. Tischuk, B. J. Marquis, K. E. H. Hartz, Secondary organic aerosol from limona ketone: Insights into terpene ozonolysis via synthesis of key intermediates, Physical Chemistry Chemical Physics 9 (23) (2007) 2991–2998. doi:10.1039/B701333G.

[22] Z. Kisiel, A. C. Legon, Conformations of some bicyclic monoterpenes based on bicyclo[3.1.0]hexane from their low-resolution microwave spectra, Journal of the American Chemical Society 100 (26) (1978) 8166–8169. doi:10.1021/ja00494a024.

[23] Z. Kisiel, O. Desyatnyk, E. Białkowska-Jaworska, L. Pszczółkowski, The structure and electric dipole moment of camphor determined by rotational spectroscopy, Physical Chemistry Chemical Physics 5 (5) (2003) 820–826. doi:10.1039/B212029A.

[24] E. M. Neeman, J. R. Avilés Moreno, T. R. Huet, The gas phase structure of α-pinene, a main biogenic volatile organic compound, The Journal of Chemical Physics 147 (21) (2017) 214305. doi:10.1063/1.5003726.

[25] E. M. Neeman, J.-R. Avilés-Moreno, T. R. Huet, The quasi-unchanged gas-phase molecular structures of the atmospheric aerosol precursor β-pinene

and its oxidation product nopinone, Physical Chemistry Chemical Physics 19 (21) (2017) 13819–13827. doi:10.1039/C7CP01298E.

[26] E. M. Neeman, P. Dréan, T. R. Huet, The structure and molecular parameters of camphene determined by Fourier transform microwave spectroscopy and quantum chemical calculations, Journal of Molecular Spectroscopy 322 (2016) 50–54. doi:10.1016/j.jms.2016.03.012.

[27] F. E. Marshall, G. Sedo, C. West, B. H. Pate, S. M. Allpress, C. J. Evans, P. D. Godfrey, D. McNaughton, G. S. Grubbs, The rotational spectrum and complete heavy atom structure of the chiral molecule verbenone, Journal of Molecular Spectroscopy 342 (2017) 109–115. doi:10.1016/j.jms.2017.09.003.

[28] J. R. Avilés Moreno, F. Partal Ureña, J. J. López González, T. R. Huet, Terpenes in the gas phase: The structural conformation of S-(–)-perillaldehyde investigated by microwave spectroscopy and quantum chemical calculations, Chemical Physics Letters 473 (1) (2009) 17–20. doi:10.1016/j.cplett.2009.03.046.

[29] M. Chrayteh, P. Dréan, T. R. Huet, Structure determination of myrtenal by microwave spectroscopy and quantum chemical calculations, Journal of Molecular Spectroscopy 336 (2017) 22–28. doi:10.1016/j.jms.2017.04.005.

[30] E. Neeman, T. R. Huet, Identification of the maze in the conformational landscape of fenchol, Physical Chemistry Chemical Physics 20 (38) (2018) 24708–24715. doi:10.1039/C8CP04011G.

[31] D. Loru, M. A. Bermúdez, M. E. Sanz, Structure of fenchone by broadband rotational spectroscopy, The Journal of Chemical Physics 145 (7) (2016) 074311. doi:10.1063/1.4961018.

[32] D. Schmitz, V. A. Shubert, T. Betz, M. Schnell, Exploring the conformational landscape of menthol, menthone, and isomenthone: a microwave study, Frontiers in Chemistry 3 (2015). doi:10.3389/fchem.2015.00015.

[33] D. Schmitz, V. A. Shubert, B. M. Giuliano, M. Schnell, The broadband microwave spectra of the monoterpenoids thymol and carvacrol: Conformational landscape and internal dynamics, The Journal of Chemical Physics 141 (3) (2014) 034304. doi:10.1063/1.4887337.

[34] M. Tudorie, L. H. Coudert, T. R. Huet, D. Jegouso, G. Sedes, Magnetic hyperfine coupling of a methyl group undergoing internal rotation: A case study of methyl formate, The Journal of Chemical Physics 134 (7) (2011) 074314. doi:10.1063/1.3554419.

[35] S. Kassi, D. Petitprez, G. Wlodarczak, Microwave spectrum of isotopic species of urea $(NH_2)_2CO$, J. Mol. Spectrosc. 228 (2) (2004) 293–297. doi:10.1016/j.jms.2004.05.002.

[36] M. J. Frisch, G. W. Trucks, H. B. Schlegel, G. E. Scuseria, M. A. Robb, J. R. Cheeseman, G. Scalmani, V. Barone, G. A. Petersson, H. Nakatsuji, X. Li, M. Caricato, A. V. Marenich, J. Bloino, B. G. Janesko, R. Gomperts, B. Mennucci, H. P. Hratchian, J. V. Ortiz, A. F. Izmaylov, J. L. Sonnenberg, Williams, F. Ding, F. Lipparini, F. Egidi, J. Goings, B. Peng, A. Petrone, T. Henderson, D. Ranasinghe, V. G. Zakrzewski, J. Gao, N. Rega, G. Zheng, W. Liang, M. Hada, M. Ehara, K. Toyota, R. Fukuda, J. Hasegawa, M. Ishida, T. Nakajima, Y. Honda, O. Kitao, H. Nakai, T. Vreven, K. Throssell, J. A. Montgomery Jr., J. E. Peralta, F. Ogliaro, M. J. Bearpark, J. J. Heyd, E. N. Brothers, K. N. Kudin, V. N. Staroverov, T. A. Keith, R. Kobayashi, J. Normand, K. Raghavachari, A. P. Rendell, J. C. Burant, S. S. Iyengar, J. Tomasi, M. Cossi, J. M. Millam, M. Klene, C. Adamo, R. Cammi, J. W. Ochterski, R. L. Martin, K. Morokuma, O. Farkas, J. B. Foresman, D. J. Fox, Gaussian 16 Rev. B.01 (2016).

[37] M. J. Frisch, M. Head-Gordon, J. A. Pople, A direct MP2 gradient method, Chemical Physics Letters 166 (3) (1990) 275–280. doi:10.1016/0009-2614(90)80029-D.

[38] M. Head-Gordon, T. Head-Gordon, Analytic MP2 frequencies without

fifth-order storage. Theory and application to bifurcated hydrogen bonds in the water hexamer, Chemical Physics Letters 220 (1) (1994) 122–128. doi:10.1016/0009-2614(94)00116-2.

[39] M. Head-Gordon, J. A. Pople, M. J. Frisch, MP2 energy evaluation by direct methods, Chemical Physics Letters 153 (6) (1988) 503–506. doi:10.1016/0009-2614(88)85250-3.

[40] M. J. Frisch, M. Head-Gordon, J. A. Pople, Semi-direct algorithms for the MP2 energy and gradient, Chemical Physics Letters 166 (3) (1990) 281–289. doi:10.1016/0009-2614(90)80030-H.

[41] H. L. Schmider, A. D. Becke, Optimized density functionals from the extended G2 test set, The Journal of Chemical Physics 108 (23) (1998) 9624–9631. doi:10.1063/1.476438.

[42] P. J. Stephens, F. J. Devlin, C. F. Chabalowski, M. J. Frisch, Ab Initio Calculation of Vibrational Absorption and Circular Dichroism Spectra Using Density Functional Force Fields, The Journal of Physical Chemistry 98 (45) (1994) 11623–11627. doi:10.1021/j100096a001.

[43] S. H. Vosko, L. Wilk, M. Nusair, Accurate spin-dependent electron liquid correlation energies for local spin density calculations: A critical analysis, Canadian Journal of Physics 58 (8) (1980) 1200–1211. doi:10.1139/p80-159.

[44] A. D. Becke, Density-functional thermochemistry. III. The role of exact exchange, The Journal of Chemical Physics 98 (7) (1993) 5648–5652. doi:10.1063/1.464913.

[45] C. Lee, W. Yang, R. G. Parr, Development of the Colle-Salvetti correlation-energy formula into a functional of the electron density, Physical Review B 37 (2) (1988) 785–789. doi:10.1103/PhysRevB.37.785.

[46] Y. Zhao, D. G. Truhlar, The M06 suite of density functionals for main group thermochemistry, thermochemical kinetics, noncovalent interactions, excited states, and transition elements: Two new functionals and systematic

testing of four M06-class functionals and 12 other functionals, Theoretical Chemistry Accounts 120 (1) (2008) 215–241. doi:10.1007/s00214-007-0310-x.

[47] T. H. Dunning, Gaussian basis sets for use in correlated molecular calculations. I. The atoms boron through neon and hydrogen, The Journal of Chemical Physics 90 (2) (1989) 1007–1023. doi:10.1063/1.456153.

[48] F. Weigend, Accurate Coulomb-fitting basis sets for H to Rn, Physical Chemistry Chemical Physics 8 (9) (2006) 1057–1065. doi:10.1039/B515623H.

[49] F. Weigend, R. Ahlrichs, Balanced basis sets of split valence, triple zeta valence and quadruple zeta valence quality for H to Rn: Design and assessment of accuracy, Physical Chemistry Chemical Physics 7 (18) (2005) 3297–3305. doi:10.1039/B508541A.

[50] R. Krishnan, J. S. Binkley, R. Seeger, J. A. Pople, Self-consistent molecular orbital methods. XX. A basis set for correlated wave functions, The Journal of Chemical Physics 72 (1) (1980) 650–654. doi:10.1063/1.438955.

[51] C. Peng, H. B. Schlegel, Combining Synchronous Transit and Quasi-Newton Methods to Find Transition States, Israel Journal of Chemistry 33 (4) (1993) 449–454. doi:10.1002/ijch.199300051.

[52] J. Laane, Determination of vibrational potential energy surfaces from raman and infrared spectra, Pure & Appl. Chem. 59 (1987) 1307–1326. doi:http://dx.doi.org/10.1351/pac198759101307.

[53] H. M. Pickett, The fitting and prediction of vibration-rotation spectra with spin interactions, Journal of Molecular Spectroscopy 148 (2) (1991) 371–377. doi:10.1016/0022-2852(91)90393-O.

[54] H. Hartwig, H. Dreizler, The microwave spectrum of trans-2, 3-dimethyloxirane in torsional excited states, Zeitschrift für Naturforschung A 51 (8) (1996) 923–932. doi:10.1515/zna-1996-0807.

[55] N. Hansen, H. Mäder, T. Bruhn, A molecular beam Fourier transform microwave study of 0-tolunitrile: 14N nuclear quadrupole coupling and methyl internal rotation effects, Molecular Physics 97 (4) (1999) 587–595. doi:10.1080/00268979909482857.

[56] O. Zakharenko, R. A. Motiyenko, J.-R. Aviles Moreno, A. Jabri, I. Kleiner, T. R. Huet, Torsion-rotation-vibration effects in the ground and first excited states of methacrolein, a major atmospheric oxidation product of isoprene, The Journal of Chemical Physics 144 (2) (2016) 024303. doi:10.1063/1.4939636.

[57] S. Bteich, M. Goubet, R. Motiyenko, L. Margulès, T. Huet, Vibrational dynamic and spectroscopic molecular parameters of trans-methylglyoxal, a gaseous precursor of secondary organic aerosols, Journal of Molecular Spectroscopy 348 (2018) 124–129. doi:https://doi.org/10.1016/j.jms.2017.12.007.

[58] A. Roucou, M. Goubet, I. Kleiner, S. Bteich, A. Cuisset, Large Amplitude Torsions in Nitrotoluene Isomers Studied by Rotational Spectroscopy and Quantum Chemistry Calculations, ChemPhysChem 21 (22) (2020). doi:10.1002/cphc.202000591.

[59] V. Van, W. Stahl, H. V. L. Nguyen, The structure and torsional dynamics of two methyl groups in 2-acetyl-5-methylfuran as observed by microwave spectroscopy, ChemPhysChem 17 (20) (2016) 3223–3228. doi:https://doi.org/10.1002/cphc.201600757.

[60] S. L. Hsu, M. K. Kemp, J. M. Pochan, R. C. Benson, W. H. Flygare, Barrier to Internal Rotation of the Methyl Group and the Identification of the trans Form of Isoprene, The Journal of Chemical Physics 50 (3) (1969) 1482–1483. doi:10.1063/1.1671221.

[61] D. R. Lide, M. Jen, Microwave Studies of Butadiene Derivatives. II. Isoprene, The Journal of Chemical Physics 40 (1) (1964) 252–253. doi:10.1063/1.1724886.

[62] D. S. Wilcox, A. J. Shirar, O. L. Williams, B. C. Dian, Additional conformer observed in the microwave spectrum of methyl vinyl ketone, Chemical Physics Letters 508 (1) (2011) 10–16. doi:10.1016/j.cplett.2011.04.001.

[63] H. S. Müller, F. Schlöder, J. Stutzki, G. Winnewisser, The Cologne Database for Molecular Spectroscopy, CDMS: a useful tool for astronomers and spectroscopists, Journal of Molecular Structure 742 (1-3) (2005) 215–227. doi:10.1016/j.molstruc.2005.01.027.